Spatially distributed infection increases viral load in a computational model of SARS-CoV-2 lung infection

Melanie E. Moses[1,2], Steven Hofmeyr[3], Judy L. Cannon[4], Akil Andrews[1], Rebekah Gridley[4], Monica Hinga[1], Kirtus Leyba[5], Abigail Pribisova[1], Vanessa Surjadidjaja[1], Humayra Tasnim[1], Stephanie Forrest[2,5]

1 Department of Computer Science, University of New Mexico, Albuquerque, New Mexico, USA
2 Santa Fe Institute, Santa Fe, New Mexico, USA
3 Lawrence Berkeley National Laboratory, Berkeley, California, USA
4 Department of Molecular Genetics and Microbiology, University of New Mexico School of Medicine, Albuquerque, New Mexico, USA
5 Biodesign Institute, Arizona State University, Tempe, Arizona, USA

Abstract

A key question in SARS-CoV-2 infection is why viral loads and patient outcomes vary dramatically across individuals. Because spatial-temporal dynamics of viral spread and immune response are challenging to study in vivo, we developed Spatial Immune Model of Coronavirus (SIMCoV), a scalable computational model that simulates hundreds of millions of lung cells, including respiratory epithelial cells and T cells. SIMCoV replicates viral growth dynamics observed in patients and shows that spatially dispersed infections lead to increased viral loads. The model shows how the timing and strength of the T cell response can affect viral persistence, oscillations, and control. By incorporating spatial interactions, SIMCoV provides a parsimonious explanation for the dramatically different viral load trajectories among patients by varying only the number of initial sites of infection, and the magnitude and timing of the T cell immune response. When the branching airway structure is explicitly represented, we find that virus spreads faster than in a 2D layer of epithelial cells, but much more slowly than in an undifferentiated 3D grid or in a well-mixed ODE model. These results illustrate how realistic spatially explicit computational models can improve understanding of within-host dynamics of SARS-CoV-2 infection.

1 Introduction

Reducing the spread, severity, and mortality caused by severe acute respiratory syndrome coronavirus 2 (SARS-CoV-2) infection is an urgent global priority. A key question is why viral loads and patient outcomes vary so dramatically among infected individuals. While severe COVID-19 disease is correlated with some known risk factors, such as age, co-morbidities, and some immune response characteristics [1–3], it remains challenging to understand why some patients develop high viral loads while others do not. We developed a scalable computational model to study the role of spatial effects in determining the time course of viral load within patients, which has been shown to affect disease severity [4] and transmission [5].

Most prior work uses Ordinary Differential Equation (ODE) models to represent within-host virus dynamics, e.g., [6–12]. Such models are useful for studying the onset and duration of the infective period [13] and the effect of various therapeutics given at different times [14–16]. However, they have limited ability to fully account for dynamics in the large and complex space of the lung [12, 17].

The Spatial Immune Model of Coronavirus (SIMCoV) is an agent-based model (ABM) that simulates infection dynamics and CD8$^+$ T cell responses in the space of hundreds of millions of epithelial cells. We highlight the importance of the spatial dispersion of virus in the lung in determining peak viral load. We focus on the T cell component of immune response because it is a key component of immunity to SARS-CoV-2. Earlier studies report that T cell levels are correlated with disease severity [18], and there is mounting evidence that T cells are critical for protection from severe illness and for preventing subsequent infection [19–22]. These studies collectively suggest that an early and strong T cell response is correlated with less severe disease, but they do not provide a quantitative understanding of how T cell response impacts viral dynamics.

Our simulations replicate viral dynamics reported from infected patients and explain differences among those patients in terms of the initial number of Foci of Infection (FOI) and the magnitude and timing of the CD8$^+$ T cell response. SIMCoV demonstrates how the spatial structure of the lung can affect viral spread in the tissue and contribute to the wide diversity of outcomes and infection dynamics observed in COVID-19 patients.

Results

SIMCoV Model Overview

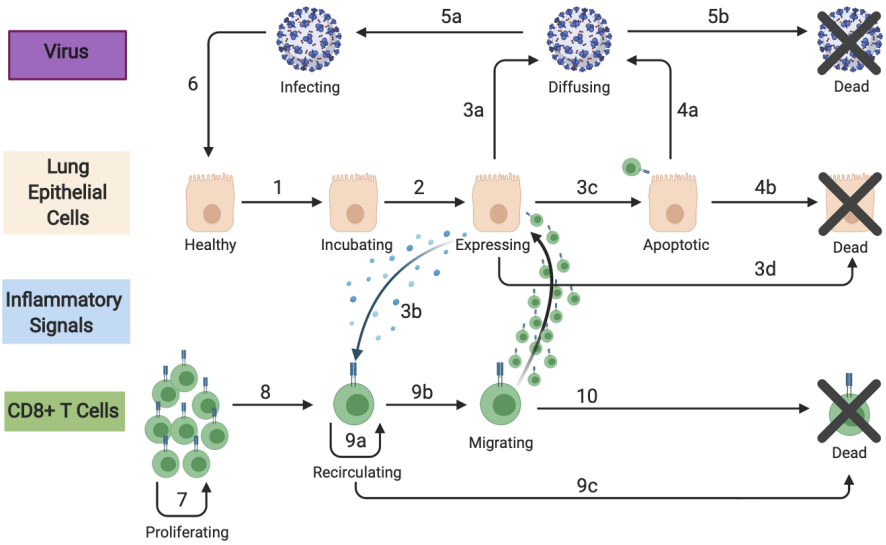

Fig 1. SIMCoV model components and their interactions. Epithelial and T cells are represented as agents; virions and inflammatory signals are represented as concentrations. Numbered transitions are described in Materials and Methods (Table 2).

SIMCoV explicitly represents virus, epithelial cells, CD8$^+$ cytotoxic T cells, and the inflammatory signals that cause T cells to extravasate into lung tissue (Fig. 1). We initialize SIMCoV with SARS-CoV-2 virus that can infect lung epithelial cells. Epithelial cells are modeled as a 2D grid, where each grid point represents a 5 x 5 x 5 μm^3 volume. Upon infection, epithelial cells incubate virus in what is often called an eclipse phase, and then they express

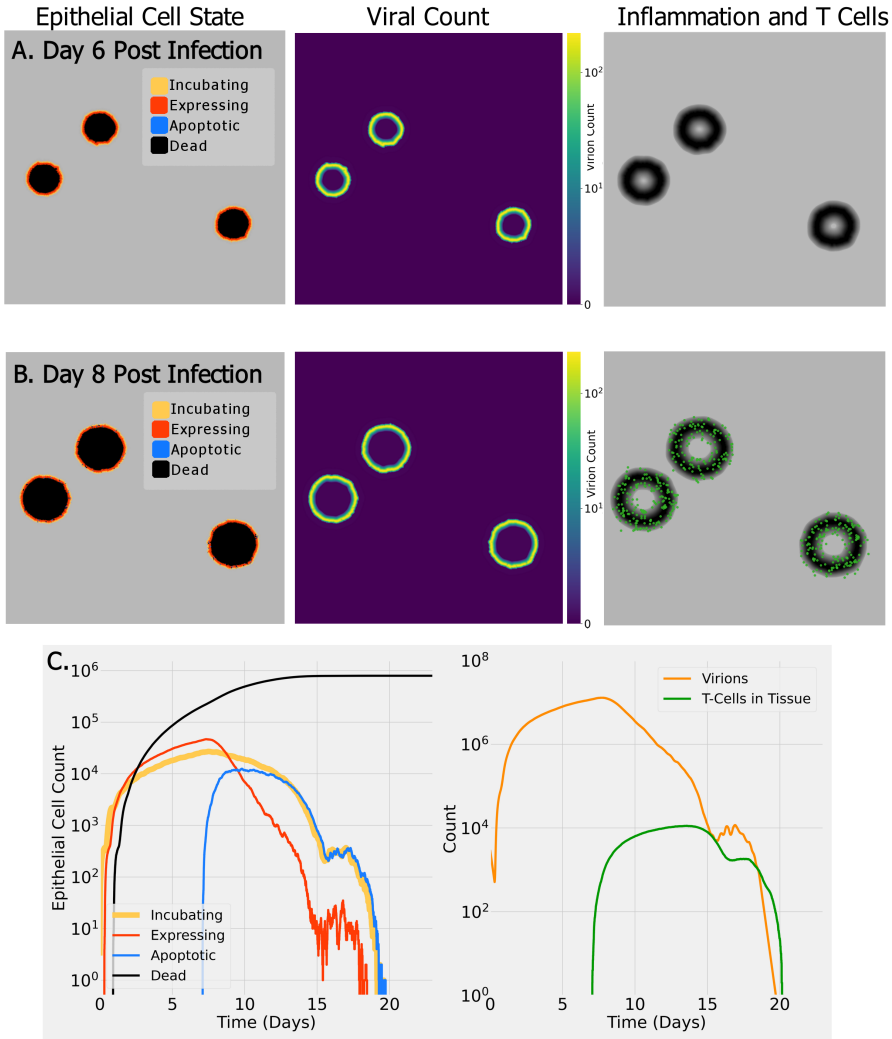

Fig 2. Example SIMCoV simulation on a 15 x 15 mm^2 layer of epithelial tissue. (a) six days post infection (dpi); (b) eight dpi. Color indicates epithelial cell state (see legend), virus concentration (see scale bar), and presence of inflammatory signal (black) and T cells (green); (c) (left panel) shows the dynamics of epithelial cell state, and (right panel) shows virus and T cell dynamics. A video demonstration of this simulation can be viewed at `https://www.youtube.com/watch?v=5K4ZSeCn-Ks`.

virus until they die. Expressing cells produce both virus and an inflammatory signal, which is an abstraction of the cytokines that influence T cell extravasation into tissue. The virus and inflammatory signal both diffuse through tissue. After seven days, we create an abstract pool representing T cells that are activated in lymph nodes and then circulate in the vasculature. When T cells reach the lung and encounter a concentration of inflammatory signal above a threshold, they extravasate and then are explicitly represented as mobile agents in SIMCoV. We adjust the probability of T cell extravasation according to the fraction of the lung that is modeled in the simulation. T cells that have extravasated move at random across the 2D grid until they either die or encounter an epithelial cell incubating or expressing virus, in which case the T cells cause apoptosis of the infected epithelial cell with some probability.

SIMCoV extends an ABM developed for influenza [23–25] by adding the ability to simulate viral spread through the 3D branching structure of lung epithelial cells and parameterizing the model for SARS-CoV-2. Each transition in Fig. 1 is parameterized with estimates or probabilities detailed in Materials and Methods and in configuration files provided with the SIMCoV code in `https://github.com/AdaptiveComputationLab/simcov`.

Fig. 2 shows the results of a run of SIMCoV with the default configuration, representing infection spreading over a 15 x 15 mm^2 layer of lung epithelial tissue (5 μm deep). The top row shows the state of epithelial cells (left), virion concentration (center), and inflammatory signal (right) at six days post infection (dpi), and the second row (Fig. 2b) shows the same including extravasated T cells at eight dpi. The dynamics of the epithelial cells, the count of virions, and the number of T cells moving through tissue are shown in the bottom row (Fig. 2c). The number of epithelial cells incubating and expressing virus (Fig. 2c, left) and viral load (Fig. 2c, right, orange line) all rise quickly after infection and then increase more slowly until seven dpi. The $CD8^+$ T cell response begins at seven dpi, and when T cells encounter infected cells, the infected cells become apoptotic. This reduces both the incubating and expressing epithelial cells and the viral load, and the cumulative number of dead cells levels off. In this example, at approximately 15 dpi, the T cells induce apoptosis in nearly all expressing epithelial cells, which leads to a reduction in produced inflammatory signals and consequently fewer T cells entering the lung. This causes the virus level to stabilize temporarily. However, once incubating and newly infected cells express more virus, more T cells enter the tissue to seek out these expressing cells and reinstate control over the infection.

Peak viral load is proportional to the number of initial FOI

We used SIMCoV to test how spatially differentiated locations of initial infection affect viral dynamics. Images of the lungs of SARS-CoV-2 patients and experimental animal models suggest that there may be multiple sites of viral infection [26, 27]. We tested the effect of seeding SIMCoV with multiple FOI on viral dynamics. We initialized simulations with one, four, and 16 spatially dispersed FOI (Fig. 3A). We find that each four-fold increase in the number of FOI increases the peak viral load (Fig. 3C) and number of extravasated T cells (Fig. 3D) by a factor of approximately four across the overall time course of infection (Fig. 3B). This remains true when the absolute number of initially infected cells is held constant across all experiments, i.e., by creating a single FOI with a cluster of 16 adjacent infected cells and four FOI with four adjacent infected cells, so that all three experiments contain 16 initially infected cells but with varying number of FOI (Fig 3C). The spatially dispersed sites act independently, so virus spreads more quickly with higher FOI because there are more infectable cells surrounding each site of infection. T cells respond by entering the tissue in greater numbers when there is more inflammatory signal produced at more sites of infection.

Effect of $CD8^+$ T cell response on viral clearance

$CD8^+$ T cells that kill virally infected cells are another key factor that varies among patients [19, 22]. The $CD8^+$ T cell response is dependent on interactions in physical space:

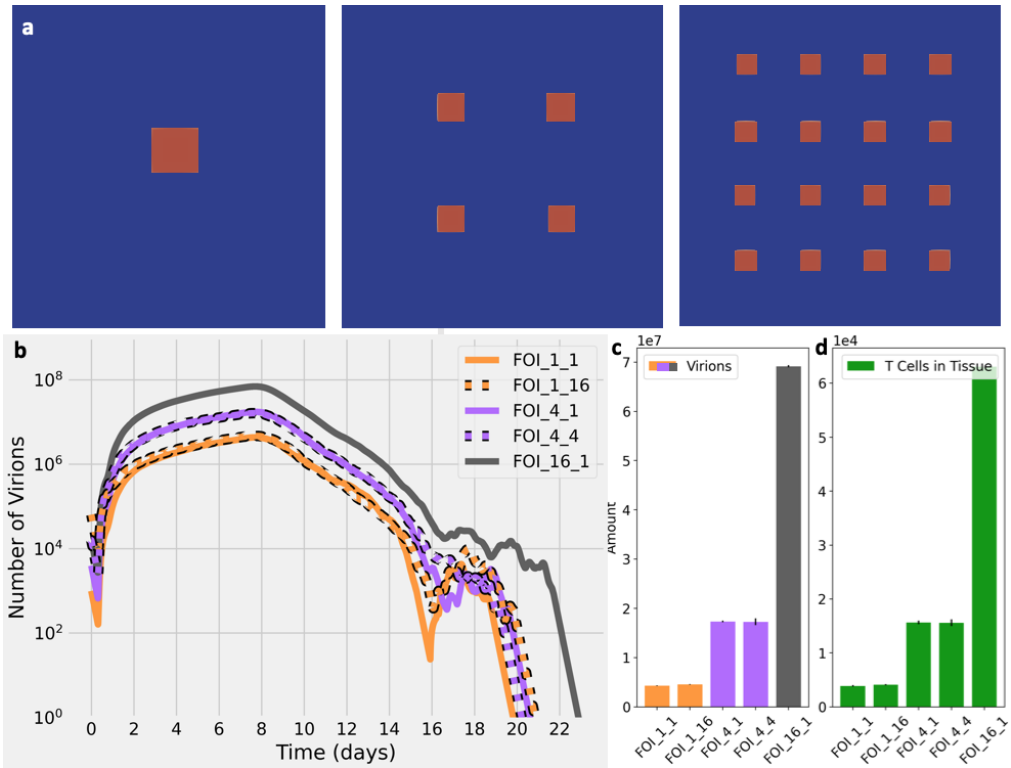

Fig 3. Effect of FOI on virus and T cell dynamics. **(a)** Initial spatial distribution in SIMCoV for one FOI (left), four FOI (center), and 16 FOI (right). **(b)** Viral load over time given different FOI. **(c)** Peak number of virions for different FOI with error bars showing the standard deviation for 10 replicates. There is a 3.90-fold increase from the one FOI configuration to the four FOI configuration and a further 3.99 increase for the 16 FOI configuration. **(d)** Peak number of T cells that extravasate into lung tissue for the different FOI. Similar to panel **(c)**, the increase is 3.95-fold for each 4-fold increase in FOI.

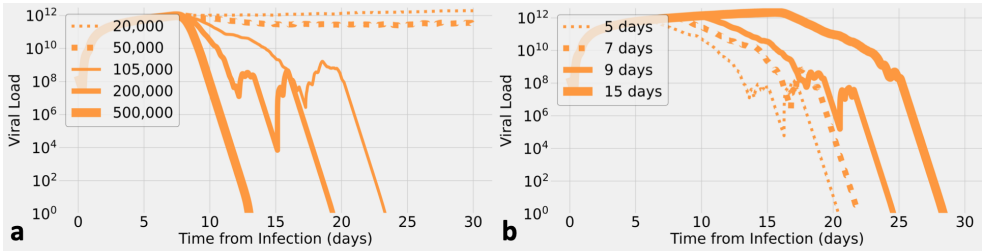

Fig 4. Effect of varying key T cell simulation parameters. (a) Effect of varying T cell generation rate when T cell delay is seven dpi; (b) effect of varying T cell delay when T cell generation rate is 105,000 T cells/min.

$CD8^+$ T cells are produced in lymph nodes, circulate in the blood and migrate to the lung, then extravasate at locations in lung tissue with inflammatory signal, and then move within infected tissue until they directly interact with infected cells to cause cell death [28–31]. T cells are likely to play an important role in controlling SARS-CoV-2 infection as elderly individuals and patients suffering from severe COVID-19 disease have fewer circulating $CD8^+$ T cells [19, 32]. However, due to technical difficulties assessing T cell responses in patients, relatively little is known about how T cell responses in the infected lung might impact viral dynamics and control.

We use SIMCoV to test how the magnitude of the T cell response affects viral control. We

Patient	T Cell Generation Rate (1000 T cells/min)	T Cell Onset (days)	Initial Sites of Infection	Viral Clearance	SIMCoV RMSLE	ODE RMLSE
A	200	8	220	0.003	1.83	1.79
B	160	7	150	0.003	2.82	2.55
C	90	5	1	0.003	2.01	2.05
D	120	6	40	0.005	2.32	1.62
E	120	10	10	0.003	3.74	3.40
F	150	9	80	0.003	2.34	1.92
G	90	6.5	50	0.004	3.58	2.88
H	160	6	3	0.004	1.31	1.82

Table 1. SIMCoV parameter settings used for each patient.

find that varying numbers of circulating T cells in the blood dramatically impacts viral control (Fig 4a). Even a 2-fold decrease in the production rate of circulating T cells can delay the timing of viral control by several days (compare solid orange lines) or even differentiate between viral control versus continued viral persistence (compare dashed orange lines to thin solid orange line).

Later $CD8^+$ T cell entry into the infected lung also delays the time it takes to reach peak viral load and allows a slightly higher peak load (Fig. 4b). Delayed T cell arrival also increases the time taken for eventual control of the infection, but it does not dramatically change the rate of reduction of viral load. Even when T cell entry into infected lung is delayed from five to 15 days, viral control can eventually be achieved, albeit later in the infection. The delay in viral control allows a longer period of elevated viral load. This may increase the window of transmission as well as tissue damage that may result in more severe disease.

SIMCoV viral loads compared to patient data

Having shown how the number of initial FOI and the timing and number of responding $CD8^+$ T cells affect viral dynamics, we next consider how these factors affect SIMCoV fits to time courses of viral load in COVID-19 patients. Following previous ODE models, e.g. [7, 8, 12, 14], we use data from sputum samples reported in Wolfel et. al. [33]. This study collected sputum from the lower respiratory tract, in contrast to most viral swabs which are collected from the nasal passage. Most of these earlier models of this data used a target cell limited (TCL) framework, in which viral load peaks when newly infectable "target" epithelial cells are depleted by previous infection. These models often predict viral loads that peak within the first four or five dpi. However, SARS-CoV-2 peak viral load occurs later in the lung than in the upper respiratory tract [34], and patient data show complex dynamics in the lung that can last 15 to 30 dpi (Fig. 5). Simple TCL models may not be as suitable for describing infection dynamics in the larger area of the lung where the epithelial lining of the branching airways and alveoli forms a large and complex surface area of up to 80 m^2 [35]. Although target cell limitation may be reached earlier in the upper respiratory tract, in the lung, it may not be achieved before the adaptive immune response begins [17].

We tested whether SIMCoV can explain the substantial variation in patient viral load data by varying only the initial FOI, T cell response, and viral clearance, which includes other immune activity. We started with the default model parameters (Materials and Methods - Table 2 and Fig. 2) and varied the number of initial sites of infection from one to 220 sites. We also varied the first day that T cells arrive in lung tissue (from five to 10 days), the T cell generation rate (from 90,000 to 200,000 cells per minute), and the viral clearance term (from 0.003 to 0.005) to account for variations in other components of the immune response.

We find that SIMCoV captures the dynamics of patient viral load over the full 25-30 day time courses with fits that are as good as those of the extended ODE described in Ke et al. [12] (Fig. 5). Table 1 shows that the goodness-of-fit is similar between SIMCoV and the ODE as measured by the Root Mean Log Squared Error (RMLSE). By varying the initial FOI, we

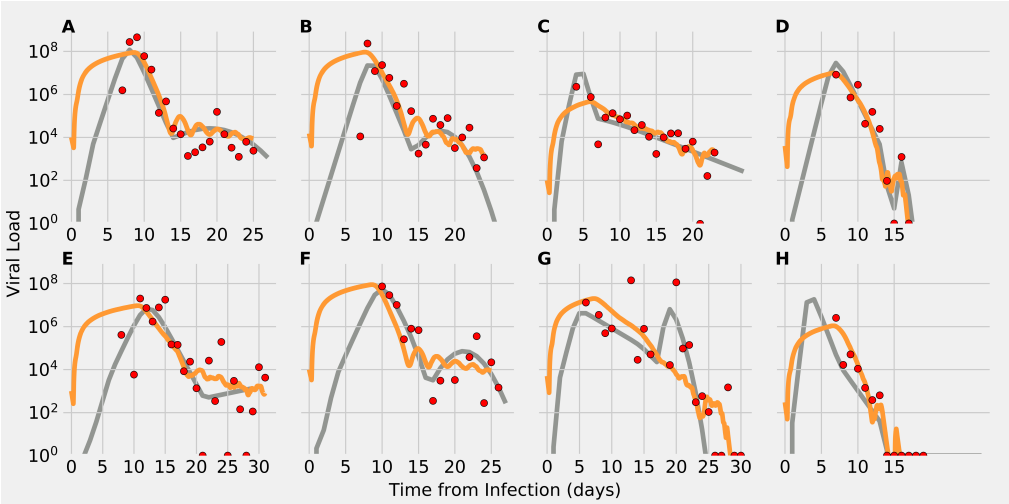

Fig 5. Viral load predictions from SIMCoV simulations (orange) compared to the extended ODE in [12] (gray), and patient data from [33] (red points).

replicate how peak viral load varies by several orders of magnitude across the eight patients. Compared to the ODE model, SIMCoV produces a less pronounced peak with higher viral loads early in infection that persist for several days. The SIMCoV curve is consistent with the observation that individuals infected with SARS-CoV-2 are most infectious early in infection before symptom onset [36, 37]. SIMCoV also predicts a longer duration of elevated viral titers, which matches patient viral load data.

Varying the T cell generation rate and first day of arrival captures the unique shapes of viral load trajectories after seven dpi. SIMCoV exhibits both oscillations in viral load and second peaks that are seen in some patients [33]. Our results support the hypothesis that decreased T cell numbers can account for viral persistence and inability to control viral load in some individuals [19, 20].

Previous TCL models have replicated the data in Wolfel et al. [33] by expanding the availability of target cells later in infection and varying many parameters in each patient [7, 12]. For example, the extended ODE model in [12] achieves good fits by varying infectivity, infected cell death rate, virion production rate, number and timing of new target cells introduced to represent newly seeded infections, and the exponential increase of the infected cell death rate to account for the adaptive immune response.

By incorporating spatial interactions, SIMCoV provides a more parsimonious explanation for the dramatically different viral load trajectories among SARS-CoV-2 positive individuals by varying only the number of FOI in the initial infection and the magnitude and timing of the immune response, particularly the T cell response. These factors are consistent with hypothesized explanations for highly variable patient outcomes. Elderly individuals have lower T cell numbers, and our model suggests that fewer T cells along with slower T cell response could help explain why elderly individuals have increased disease severity [19, 22]. More speculatively, the number of FOI could increase with a larger inhaled viral innoculum, a factor that Gandhi et. al. [38] suggest would increase disease severity. Variation in FOI and T cell response may also account for the long infectious period in some patients [4–6].

Modeling viral spread over branching airways

The SIMCoV experiments described above simulate a single layer of epithelial cells (Figs. 2, 3, 4, 5). However, the lung is a highly complex structure of branching airways descending from large bronchioles down to alveoli lined by epithelial cells, with much of the volume consumed

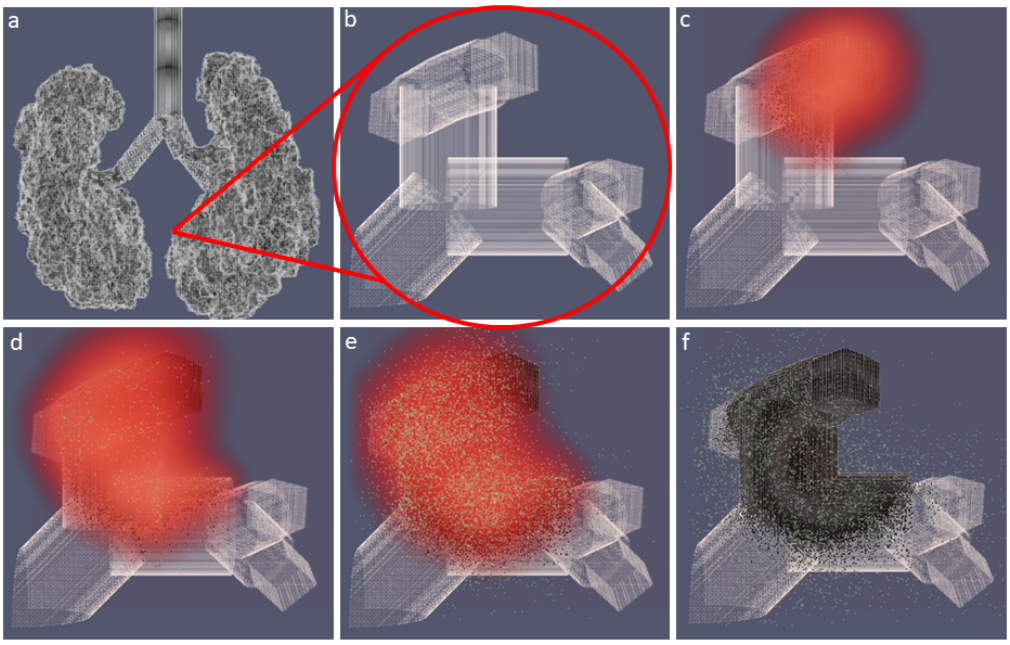

Fig 6. Simulated 3D branching airway with a single FOI. **(a)** shows the full lung model; **(b)** - **(f)** show T cells (green), virions (red) and a small region of epithelial cells (gray) at **(b)** 0 dpi, **(c)** 4.2 dpi, **(d)** 6.3 dpi, **(e)** 6.9 dpi, and **(f)** 8.3 dpi. Dead epithelial cells are indicated in black. A video corresponding to these images is available at `https://youtu.be/WbiLH9NRfbA`.

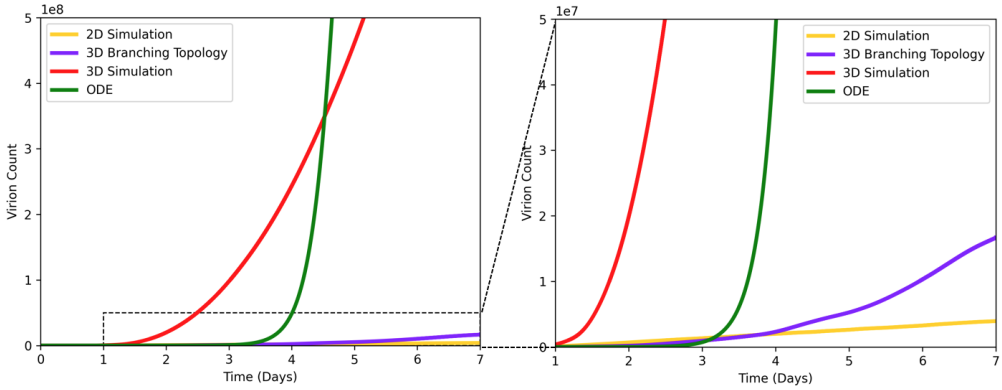

Fig 7. Viral spread given different model topologies. Virion count is plotted vs. time for four different SIMCoV configurations: 2D grid (yellow); 3D grid (red); 3D branching model (purple); ODE model (green). The right panel is zoomed in on the y-axis (showing up to 10^7 virions) to show the dotted region of the left panel (which shows up to 10^8 virions). Each simulation was run with sufficient numbers of epithelial cells that they do not reach target cell limitation.

by alveolar space for gas exchange [35]. To investigate whether the lung airway structure impacts viral spread and T cell control, we developed a bifurcating fractal branching algorithm and integrated it into SIMCoVsimulations to form the surface of the epithelial layer. Following Yeh et. al [39], we model 26 branching generations (from the trachea to alveolar sacs) in all five lobes of the lung. The 3D branching model incorporates trachea, bronchi, bronchioles, and ducts, represented as cylinders of epithelial cells with length, diameter, branching angle, and gravity angle calculated at each level of the branching hierarchy, and each terminal alveolar sac is represented as a hollow 200 x 200 x 200 μm^3 cube of epithelial cells. Fig. 6a shows the full

model of the branching structure, and Figs. 6b-f show how virus spreads over a small region of bronchioles and alveoli in a 1500 x 1500 x 1500 μm^3 volume.

Fig. 7 shows how the topology of epithelial cells modeled in SIMCoV affects the predicted rate of viral spread in the first seven dpi and before the T cell response. The branching network model (Fig. 6) best captures the spatial arrangement of epithelial cells. Viral spread over the branching network (purple line in Fig. 7) shows only four times greater growth than the simple 2D layer (yellow line) that we used in our earlier simulations. In contrast, an undifferentiated 3D grid of cells (red line) generates 66 times more infected cells than the branching model at the end of the first week of infection, and the TCL ODE from [12] (green line) generates thousands of times more infected cells before reaching target cell limitation within the first week.

We hypothesize that the 2D model slightly underestimates viral growth because it is constrained by the circumference of the circle of infection which grows linearly with the total number of cells in the FOI (Fig. 2). In (non-branching) 3D grid simulations, infection spreads from the faster growing sphere of infected cells. ODE models assume all infected cells can infect all other infectable cells, and without spatial constraints, the virus spreads even faster. At least at the scale of hundreds of millions of cells that we model here, the simple 2D model captures the dynamics of the branching model well. In future work we will consider more detailed movement of virus and immune cells through the epithelium and branching airways as well as the percent and locations of infectable cells in simulations at the full scale of the human lung.

Discussion

SIMCoV models the spread of SARS-CoV-2 through the lung and subsequent immune control by T cells. Results from our spatial model complement earlier well-mixed ODE models but make different predictions. For example, the earlier models predict a sharp early peak in viral load in the first few days of infection, while SIMCoV predicts a broader peak which rises rapidly for the first few days post-infection and then continues to increase slowly until the T cell response begins between day seven and 10 [40]. Viral levels then decline gradually but continue to oscillate as infected cells continue to produce virus and as T cells discover pockets of hidden infection. The viral load dynamics predicted by SIMCoV are consistent with observations that the viral load in the lung peaks later than in the upper respiratory tract and can persist for much longer [16, 17, 41]. SIMCoV simulations suggest that variable spatial seeding of virus in multiple FOI is a key factor accounting for the highly heterogeneous viral loads observed in patients.

SIMCoV and other ABM are appealing because they can represent and visualize the complex heterogeneous movements of individual cells and diffusing fields of small particles (i.e. virions or cytokines) [42]. Our prior results showed how key factors such as spread of infection, molecules, and cells affect search efficiency, timing of immune response initiation, and successful clearance of infection, and that interactions that depend on movement and physical cell-cell contact require a spatially-explicit modeling framework [25, 43]. SIMCoV simulation of SARS-CoV-2 reinforces the importance of spatial effects as drivers of viral dynamics in the lung.

Some earlier SARS-CoV-2 ODE TCL models included an implicit immune response incorporated in the cell clearance term and an explicit adaptive immune response, e.g. [8, 14–16, 44], similar to the approach we took with SIMCoV. These models were tuned to fit the same lung viral load data from [33] that we fit here; however, because SIMCoV explicitly represents cell and virus movement, it mimics the highly variable dynamics by varying only a few key parameters. Specifically, varying T cell arrival time by only a few days (from five to 10 dpi, consistent with [40]) and the magnitude of the T cell and other immune responses by two-fold accounts for the variability and oscillations in viral clearance of the patients from [33] (Fig. 5). This is consistent with studies that show $CD8^+$ T cells in particular are critical for clearance and control of SARS-CoV-2 infection [18, 19, 22, 45, 46].

T cell killing of infected cells requires direct cell to cell contact [28, 30, 47]. Because SIMCoV represents spatial positioning and T cell movement explicitly, their physical

co-location with infected cells arises naturally in the model. This modeling strategy provides a mechanistic explanation, which shows how even a small decrease in the number of responding T cells changes viral dynamics from a smooth decline to an oscillating decline to uncontrolled viral persistence. Interestingly, later arrival of T cells into the infected lung delays viral control but otherwise has little affect on viral dynamics or clearance. Although we do not explicitly model other important aspects of immune response to SARS-CoV-2, for example, Type I interferons, other innate responses, and antibody responses, SIMCoV accounts for these effects in the viral clearance term. Future studies using SIMCoV could explicitly represent these additional immune parameters.

While good fits to patient data were achieved with only small amounts of variation in T cell generation rates and timing, achieving good fits to patient peak viral load requires a much larger range of variation in FOI, from one to 220. In our analysis, the number of FOI within the lung is the key driver of peak viral load, and accounting for it requires a spatially explicit modelling framework. An important insight from SIMCoV is that spatial dispersion of virus may be particularly important for SARS-CoV-2 and other lung infections because the epithelial surface area of the lung is so large. In contrast to the smaller surface areas of the nasopharynx, where TCL can be reached very quickly regardless of how much initial virus is inhaled, viral spread through the larger area of the lung takes more time [17].

We find that the number of initial FOI in the lung determines how fast the virus spreads and how high a peak it reaches, but the the actual number of virions causing initial infection does not independently affect the viral peak (Fig. 4). However, in real infections, if more virus is inhaled, the likelihood of virus taking hold in more FOI may increase, so the number of infective virions and the spatial dispersion of those virions may be correlated. High variability in how much virus individual patients inhale and how dispersed that virus is in the lung may be an important contributor to the large variation in viral load and disease outcome in demographically similar patients.

Spatial simulations in SIMCoV also allowed us to test how the branching topology of the lung might impact viral spread in the lower respiratory tract. Our results show that the geometry of lung tissue has substantial effect on the rate of viral spread (Fig. 7). Surprisingly, of the models we considered, the more realistic model with epithelial cells lining the branching airways produced dynamics most similar to the 2D model with epithelial cells arranged in a simple grid. In contrast, the 3D and ODE models both predict much faster viral growth than the branching model. In fact, ODE models with TCL require extremely fast viral growth (e.g., $R_0 \approx 27$ in [12]) to reach TCL (in which all infectable cells are infected) and fit to the timing of the viral peak. In our SIMCoV simulations, virus spread more slowly because it is constrained by the spatial topology of the epithelium, while target cell limitation is not reached. Thus, our spatial model hypothesizes that viral control arises from the immune response (specifically the CD8+ T cell response), rather than the virus infecting all infectable cells. Our hypothesis that not all lung cells are infected is consistent with observed mild or moderate illness of many patients, including those in [33]. It is also consistent with CT scans that show tissue damage in only a small percentage of tissue early in infection [48]. Thus, by representing spatial constraints on viral spread, SIMCoV suggests a different mechanism for viral control than previous models that did not consider spatial effects.

Previous spatially explicit models were limited both by data on infection dynamics and the computational power to explicitly represent spatial interactions among large numbers of of cells [42]. SIMCoV overcomes these limitations by leveraging the data shared in response to the COVID-19 pandemic and an underlying architecture that takes advantage of HPC capabilities. The SIMCoV platform could be used to simulate other spatial interactions such as predator prey dynamics between immune and infected cells or collective action dynamics [11], such as the collective search strategies of T cells [49].

To enable open and reproducible science, SIMCoV is freely available under an open-source license, and it was designed to be easily extensible. Future extensions of the model can scale up

to full lung size, investigate the effects of mucus and the complex dynamics of airflow in the respiratory tract [50], and include more detailed topological models of the airways and alveoli and the fraction and distribution of epithelial cells with receptors necessary for infection. SIMCoV can also explicitly incorporate additional aspects of the innate and adaptive immune response. By predicting the time course of viral loads within individuals, SIMCoV can help to identify factors that determine windows of transmission between individuals and thereby improve understanding of epidemic spread.

Materials and Methods

Model Description

SIMCoV[1] is an Agent Based Model (ABM) where space is represented by a discrete Cartesian grid, which can be either two or three-dimensional. For clarity, we describe the model with reference to a 2D layer of epithelial cells, although the mechanisms apply equally to other topologies such as 3D simulations that include the branching structure of lung airways.

The grid points are spaced five microns apart (roughly the diameter of a T cell), and components of the model only exist at these discrete locations. The model is run as a discrete-time simulation, where each time step represents one minute, approximately the time it takes for a T cell to move five microns (one grid point) [31, 51]. At each time step, the model components are updated according to their states and interactions.

There are four main components of SIMCoV: epithelial cells, $CD8^+$ T cells, virions, and inflammatory signals, representing the subset of cytokines that cause T cell extravasation into the lung tissue. The interactions between these components are shown in Fig. 1. Each epithelial cell has a fixed grid location with no more than one cell per location. However, some locations can be empty, representing airways (as can be seen in Fig. 6). In addition, a single T cell may also occupy a grid point, and every grid point can have a concentration of virions and inflammatory signals. The number of virions is represented explicitly and is capped at 125,000 virions, which is the maximum number estimated to fit within five μm^3. The concentration of inflammatory signal is represented as a floating point number between 1×10^{-6} and one.

Each simulation run begins with a number of sites of infection (parameter **b** in Table 2), which are grid points with an initial level of virions (parameter **c**). At each time step, the virions will diffuse uniformly at a given rate (parameter **j**) to neighboring grid points, both those with and without epithelial cells, and some fraction (parameter **i**) of the virions will be cleared, reducing the concentration.

Initially, epithelial cells are *healthy* (not infected), but all are able to be infected. At the end of a time step, if there are virions in the same location as a healthy epithelial cell, that cell will become infected (transition **1** in Fig. 1) with a probability proportional to the virion concentration, multiplied by the *infectivity* (parameter **g**). An infected epithelial cell is initially in an *incubating* state, in which it remains for a period of time defined by the mean of a Poisson distribution (parameter **d**)[2], after which it transitions to an *expressing* state (transition **2**). An epithelial cell that is *expressing* will produce virions at a constant rate per time step (parameter **h**, transition **3a**), and those will be added to the local concentration and diffuse outwards (transition **4a**) and be cleared (transition **4b**). In the absence of a T cell response, after a further time period (parameter **e**), an *expressing* cell will transition to the *dead* state (transition **3c**).

When epithelial cells are *expressing* (and *apoptotic* - described below), they will produce inflammatory signals at a constant rate (parameter **k**) per time step (transition **3b**). Those signals will diffuse to neighboring grid points and decay at constant rates (parameters **m** and **l**, respectively). The concentration of inflammatory signal is represented as a floating point

[1] The source code for SIMCoV is publicly available at `https://github.com/AdaptiveComputationLab/simcov`.

[2] Parameters that are time periods are all Poisson distributions specified by the mean.

Parameter	Description	Default	Reference
a) Dimensions	Simulation size in x,y, and z dimensions	15000x15000x1	*
b) Initial Infections	Number of grid points with initial infections	1	*
c) Initial Virions	Number of virions at initial infection locations	1000	*
d) Incubation Period	Average minutes until an infected cell starts expressing virions	480	[52]
e) Expressing Period	Average minutes after expressing starts until cell death	900	[10]
f) Apoptosis Period	Average minutes after apoptosis is induced until cell death	180	[53]
g) Infectivity	Probability of one virion infecting one cell per minute	0.001	[25]
h) Virion Production	Number of virions produced by expressing cell per minute	1.1	[54]
i) Virion Clearance	Fraction by which virion count drops per minute	0.004	[25]
j) Virion Diffusion	Fraction of virions that diffuse into all neighboring grid points per minute	0.15	[25]
k) Inflammatory Signal Production	Concentration of inflammatory signal produced by expressing cells per minute	1	*
l) Inflammatory Signal Decay	Fraction by which inflammatory signal concentration drops per minute	0.01	*
m) Inflammatory Signal Diffusion	Fraction of inflammatory signal that diffuses into all neighboring grid points per minute	1	[25]
n) T Cell Production	Number of T cells generated per minute into circulation	105000	[25, 55]
o) T Cell Initial Delay	Average minutes before T cells start to be produced	10080	[40, 56, 57]
p) T Cell Vascular Period	Average minutes before death for a T cell in the vasculature	5760	[25]
q) T Cell Tissue Period	Average minutes before death for a T cell after it extravasates	1440	[58]
r) T Cell Binding Period	Average minutes T cell is bound to an epithelial cell	10	[30]

Table 2. Table of SIMCoV parameters. The default values represent the COVID-19 parameters we collected from a variety of sources. Time periods are Poisson distributions, defined by the average. One time step is one minute, and grid points are five microns apart. Unless stated otherwise, the default parameters were used for all experiments. Parameters marked with (*) were not taken from the literature—see Parameter Derivation.

number with a minimum value (1×10^{-6}), so that, eventually, it will be completely eliminated if there is no more being added by infected cells. In the current implementation of SIMCoV, the inflammatory signal serves only as a trigger for T cell extravasation, but it can easily be extended to represent other chemokines and cytokines in future work.

It is assumed that after an initial delay (parameter **o**), activated antigen-specific $CD8^+$ T cells begin to enter the blood from lymph nodes (transition **7**) at a constant rate (parameter **n**). T cells in the vasculature extravasate into lung tissue when they detect inflammation (transition **9b**). T cell movement through the vasculature is not explicitly modeled; instead, a random location is chosen for each T cell at every time step, and if that location contains an inflammatory signal, then the T cell extravasates. The random location is chosen from among all of the possible locations for a full-sized lung, so if only a fraction of the lung is being modeled, then the probability of extravasation is reduced accordingly. Only one T cell can occupy a location in the tissue at a time, so a T cell will not extravasate to a location already occupied by another T cell. T cells that do not extravasate continue to circulate in the vasculature (transition **9a**), and those that fail to extravasate before the vascular T cell lifespan (parameter **p**) will die and be removed from the simulation (transition **9c**).

A T cell that is in the tissue can potentially bind to an epithelial cell that is at the same or a neighboring location (transition **10a**). The probability of binding is proportional to the period the cell has been incubating, with a maximum of one if the cell is expressing. Multiple T cells can bind to a single infected cell, providing they are neighbors or colocated with the infected cell. When a T cell binds to an epithelial cell, the latter transitions to the *apoptotic* state (transition **3d**) and after a given time period (parameter **f**), it dies (transition **6b**). Apoptotic epithelial cells continue to produce virions (transition **6a**) and inflammatory signals at the same rates as expressing cells. T cells remain bound for a fixed time period (parameter **r**), after which they move in the tissue, at every time step moving to a randomly selected neighboring location that does not already contain a T cell. Hence, T cells move at maximum rate of five microns per minute [31]. If after moving, a T cell finds itself a neighbor of or colocated with an infected cell, it once again can bind. This process of random movement and possible binding continues until the T cell dies (transition **10b**) after a certain time period (parameter **q**). T cells in the tissue never return to the vasculature.

Parameter Derivation

Where possible, parameter settings were derived from a close investigation of available data, as described here:

a. *Dimensions*: in general, set to a sufficiently large size so that a simulation will not induce target cell limitation in the first week of infection; for the default 2D simulation, the z-dimension will be one.

b. *Initial Infections*: set to one to represent the minimum number of infected locations in the lower respiratory tract.

c. *Initial Virions*: set according to the *infectivity* parameter (**g**) in order to successfully infect at least one cell initially.

d. *Incubation Period*: roughly the eclipse period; estimated to be 7-8 hours or 480 time steps in [52].

e. *Expressing Period*: estimated to be about 15 hours or 900 minutes in [10], which is similar to the expressing period of the influenza virus (about 1000 minutes [25]).

f. *Apoptosis Period*: estimated to range between 48 minutes and 168 minutes in mice [53]; we estimate a slightly longer period, 180 minutes, for humans.

g. *Infectivity*: set to 0.001, which is the probability of infection per cell per minute, i.e. it will take on average 1,000 minutes for a virion to infect a cell. This is within the range of 12 to 1,200 minutes estimated for influenza [25]. This is a largely unknown value that will vary between diseases and disease strains.

h. *Virion Production*: calculated by dividing the burst size by the expressing period (**e**); the burst size is the total virions produced by an infected cell, which was found to be 1,000 virions [54].

i. *Virion Clearance*: set to 0.004 virions per minute, which is within prior calculations of the virion decay rate of the influenza virus, ranging from 7e-7 to 0.07 virions per minute [25]. We vary this parameter from 0.003 to 0.005 to fit patient data.

j. *Virion Diffusion*: this is calculated from the Einstein-Smoluchowski equation for particle movement, $D \approx \alpha.x^2/(2t)$, where x is the mean distance diffused in one direction along one axis in time t, and α is the SIMCoV parameter. Hence, for a mean distance of five microns (one grid point), a time of one minute (one simulation time step), and a virion diffusion parameter of 0.15, the diffusion coefficient is $0.0312\mu m^2/s$. This diffusion coefficient is similar to the diffusion coefficient calculated for influenza [25], which is $0.0318\mu m^2/s$.

k. *Inflammatory Signal Production*: the concentration of inflammatory signal produced per minute is not explicitly expressed in literature; therefore, we provide an estimate and modify it to best fit published viral data.

l. *Inflammatory Signal Decay*: there are no explicit measurements of this value in the literature; we estimate a half life of 70 minutes, which is similar to the half life of 30 minutes estimated as plausible for influenza [25].

m. *Inflammatory Signal Diffusion*: calculated from the Einstein-Smoluchowski equation for particle movement, $D \approx \alpha.x^2/(2t)$, where x is the mean distance diffused in one direction along one axis in time t, and α is the SIMCoV parameter. Hence, for a mean distance of five microns (one grid point), a time of one minute, and a inflammatory signal diffusion parameter of 1, the diffusion coefficient is $0.210\mu m^2/s$, which is within the range of the chemokine diffusion coefficient calculated in [25] (from $0.00318\mu m^2/s$ to $318\mu m^2/s$).

n. *T Cell Production*: the number of T cells produced by replication in the mediastinal lymph nodes of the lung is calculated by scaling up the T cell production rate in Levin et al. [25], which was estimated from mouse models [55]. That previous calculation assumed that a single virus-specific T cell encounters an antigen presenting cell and begins to replicate on day 0 post infection, doubling every eight hours. After five days, those activated CD8+ T cells could generate approximately 30,000 new T cells per day (or 21 per minute) into circulation. In this current SIMCoV model, we assume a linear 5,000-fold increase from mouse to human, which reflects the approximate increase in lung and blood volume and gives a rate of 105,000 T cells per minute entering circulation.

o. *T Cell Initial Delay*: estimated from [40] for SARS-CoV-2. Our default time is seven dpi, and we vary from five to ten dpi to fit patient data. We note that if T cells double every eight hours and replication in humans lasts 2.3 days longer than in mice (seven versus five dpi), this would cause a 128-fold increase in T cell production. With 40 times greater SARS-CoV-2 specific T cell precursors, this would generate 5,000 times greater T cell production in humans. Alternatively, exponential replication of a single T cell precursor for nine days would generate 5,000 times greater production in humans compared to mice.

p. *T Cell Vascular Period*: equivalent to the T cell age in the blood for a model of T cell responses to influenza [25].

q. *T Cell Tissue Period*: largely unknown, but estimates were provided in Keating et al. [58].

r. *T Cell Binding*: taken from Halle et al. [30].

Model Implementation

The SIMCoV model is implemented in UPC++ [59], which is a high performance language for parallel computation that runs on a variety of platforms, including distributed memory supercomputers and networked clusters. Consequently, the SIMCoV application can run on systems from laptops up to high performance supercomputers without requiring any code changes. However, because of the computational cost of the simulation, only small areas can be simulated on smaller systems with one or a few compute nodes. Simulations of significant fractions of the human lung requires hundreds or thousands of compute nodes.

Massively Parallel Simulation

SIMCoV is designed by the composition of highly parallelizable functions to make a highly scalable simulation framework. Running immense agent-based simulations of this type would not be computationally feasible without the application of high performance computing techniques (HPC). For SIMCoV, we rely on the HPC primitives and multi-process communication techniques provided by UPC++, a library extension to the C++ programming language with state-of-the-art HPC capabilities [59]. We reduce the communication and computational work load of running large SIMCoV simulations with different approaches. To mitigate expensive cross process calculation, we maintain three-dimensional or two-dimensional blocks of closely spaced grid points in contiguous single process memory. This lowers the chance that for any given update of agents in the simulation that two processes have to share memory. To prevent unnecessary computation costs, we maintain an *active list* of agents and grid points that will be updated at each iteration of the simulation. Some grid points can be predicted to remain constant from one iteration to the next, so there is no need to update their behavior for that step.

SIMCoV can be used to run large simulations in minutes on suitable supercomputers. For example, we simulated an infection seeded with multiple initial FOI in 285000 x 285000 x 5 μm^3 tissue, comprising over three billion epithelial cells, which is equivalent to a single slice of tissue through the full human lung. On the NERSC Cori supercomputer, it took 15 minutes to complete a two week simulation on 32 nodes.

ODE Model Implementation

Our ODE implementation was taken from the model in [12], which was fit to the published sputum swab viral load data of nine infected individuals over 14-28 days [33]. We used the version of their model that describes viral dynamics over the first days of infection prior to adaptive immune response. Most parameters are similar to our SIMCoV parameters, such as the virion clearance rate or virion production rate. We implemented this ODE model using the scipy odeint Python package, the model description in [12], and the fit model parameters for patient A in [12].

Acknowledgements

We thank Ruian Ke for sharing insights and an early draft of his ODE model; Matthew Fricke, UNM CARC, and ASU RC for HPC resources and support; and Greg Forest for many helpful discussions. This project was funded by NSF 2030037 and 2029696 which includes Coronavirus Aid, Relief, and Economic Security (CARES) Act funding. DARPA provided partial funding

through AFRL FA-8650-18-C-6898 (JLC, MM, HT and AA).This work is also partly supported by the Advanced Scientific Computing Research (ASCR) program within the Office of Science of the DOE under contract number DE-AC02-05CH11231 (SH); Exascale Computing Project (17-SC-20-SC), a collaborative effort of the U.S. Department of Energy Office of Energy (SH). We used resources of the NERSC supported by the Office of Science of the DOE under Contract No. DEAC02-05CH11231. **Author Contributions:** M.E.M., S.F., J.L.C. and S.H. conceived the study. S.H. designed and coded the model, S.H., A.A., R.G., M.H., K.L., A.P. V.S. and H.T. ran the models, assembled data, performed calculations, and analyzed output. M.E.M, S.F., J.L.C. and S.H. wrote the manuscript with contributions from all other authors.

References

1. Moderbacher CR, Ramirez SI, Dan JM, Grifoni A, Hastie KM, Weiskopf D, et al. Antigen-specific adaptive immunity to SARS-CoV-2 in acute COVID-19 and associations with age and disease severity. Cell. 2020;183(4):996–1012.
2. Arunachalam PS, Wimmers F, Mok CKP, Perera RA, Scott M, Hagan T, et al. Systems biological assessment of immunity to mild versus severe COVID-19 infection in humans. Science. 2020;369(6508):1210–1220.
3. Yang J, Zheng Y, Gou X, Pu K, Chen Z, Guo Q, et al. Prevalence of comorbidities and its effects in patients infected with SARS-CoV-2: a systematic review and meta-analysis. International Journal of Infectious Diseases. 2020;94:91–95.
4. Fajnzylber J, Regan J, Coxen K, Corry H, Wong C, Rosenthal A, et al. SARS-CoV-2 viral load is associated with increased disease severity and mortality. Nature Communications. 2020;11(1):1–9. doi:10.1038/s41467-020-19057-5.
5. Marks M, Millat-Martinez P, Ouchi D, h Roberts C, Alemany A, Corbacho-Monné M, et al. Transmission of COVID-19 in 282 clusters in Catalonia, Spain: a cohort study. The Lancet Infectious Diseases. 2021;.
6. Néant N, Lingas G, Le Hingrat Q, Ghosn J, Engelmann I, Lepiller Q, et al. Modeling SARS-CoV-2 viral kinetics and association with mortality in hospitalized patients from the French COVID cohort. Proceedings of the National Academy of Sciences. 2021;118(8).
7. Wang S, Pan Y, Wang Q, Miao H, Brown AN, Rong L. Modeling the viral dynamics of SARS-CoV-2 infection. Mathematical biosciences. 2020;328:108438.
8. Hernandez-Vargas EA, Velasco-Hernandez JX. In-host mathematical modelling of covid-19 in humans. Annual reviews in control. 2020;.
9. Gonçalves A, Bertrand J, Ke R, Comets E, De Lamballerie X, Malvy D, et al. Timing of antiviral treatment initiation is critical to reduce SARS-CoV-2 viral load. CPT: pharmacometrics & systems pharmacology. 2020;9(9):509–514.
10. Kim KS, Ejima K, Ito Y, Iwanami S, Ohashi H, Koizumi Y, et al.. Modelling SARS-CoV-2 dynamics: Implications for therapy; 2020.
11. Metcalf CJE, Grenfell BT, Graham AL. Disentangling the dynamical underpinnings of differences in SARS-CoV-2 pathology using within-host ecological models. PLoS pathogens. 2020;16(12):e1009105.
12. Ke R, Zitzmann C, Ribeiro RM, Perelson AS. Kinetics of SARS-CoV-2 infection in the human upper and lower respiratory tracts and their relationship with infectiousness. medRxiv. 2020;.
13. Ejima K, Kim KS, Ludema C, Bento AI, Iwanami S, Fujita Y, et al. Estimation of the incubation period of COVID-19 using viral load data. Epidemics. 2021;35:100454.
14. Goyal A, Cardozo-Ojeda EF, Schiffer JT. Potency and timing of antiviral therapy as determinants of duration of SARS-CoV-2 shedding and intensity of inflammatory response. Science advances. 2020;6(47):eabc7112.
15. Kim KS, Ejima K, Iwanami S, Fujita Y, Ohashi H, Koizumi Y, et al. A quantitative model used to compare within-host SARS-CoV-2, MERS-CoV, and SARS-CoV dynamics provides insights into the pathogenesis and treatment of SARS-CoV-2. PLoS biology. 2021;19(3):e3001128.

16. Perelson AS, Ke R. Mechanistic modelling of SARS-CoV-2 and other infectious diseases and the effects of therapeutics. Clinical Pharmacology & Therapeutics. 2020;.

17. Du SQ, Yuan W. Mathematical modeling of interaction between innate and adaptive immune responses in COVID-19 and implications for viral pathogenesis. Journal of medical virology. 2020;92(9):1615–1628.

18. Zhang X, Tan Y, Ling Y, Lu G, Liu F, Yi Z, et al. Viral and host factors related to the clinical outcome of COVID-19. Nature. 2020;583(7816):437–440.

19. Sette A, Crotty S. Adaptive Immunity to SARS-CoV-2 and COVID-19. Cell. 2021;doi:https://doi.org/10.1016/j.cell.2021.01.007.

20. Tan AT, Linster M, Tan CW, Le Bert N, Chia WN, Kunasegaran K, et al. Early induction of functional SARS-CoV-2-specific T cells associates with rapid viral clearance and mild disease in COVID-19 patients. Cell reports. 2021;34(6):108728.

21. Grifoni A, Weiskopf D, Ramirez SI, Mateus J, Dan JM, Moderbacher CR, et al. Targets of T cell responses to SARS-CoV-2 coronavirus in humans with COVID-19 disease and unexposed individuals. Cell. 2020;181(7):1489–1501.

22. Bertoletti A, Tan AT, Le Bert N. The T-cell response to SARS-CoV-2: kinetic and quantitative aspects and the case for their protective role. Oxford Open Immunology. 2021;2(1).

23. Warrender C, Forrest S, Koster F. Modeling intercellular interactions in early Mycobacterium infection. Bulletin of mathematical biology. 2006;68(8):2233–2261.

24. Mitchell H, Levin D, Forrest S, Beauchemin CA, Tipper J, Knight J, et al. Higher level of replication efficiency of 2009 (H1N1) pandemic influenza virus than those of seasonal and avian strains: kinetics from epithelial cell culture and computational modeling. Journal of virology. 2011;85(2):1125–1135.

25. Levin D, Forrest S, Banerjee S, Clay C, Cannon J, Moses M, et al. A spatial model of the efficiency of T cell search in the influenza-infected lung. Journal of Theoretical Biology. 2016;398. doi:10.1016/j.jtbi.2016.02.022.

26. Imai M, Iwatsuki-Horimoto K, Hatta M, Loeber S, Halfmann PJ, Nakajima N, et al. Syrian hamsters as a small animal model for SARS-CoV-2 infection and countermeasure development. Proceedings of the National Academy of Sciences. 2020;117(28):16587–16595.

27. Zhang K, Liu X, Shen J, Li Z, Sang Y, Wu X, et al. Clinically applicable AI system for accurate diagnosis, quantitative measurements, and prognosis of COVID-19 pneumonia using computed tomography. Cell. 2020;181(6):1423–1433.

28. Harris TH, Banigan EJ, Christian DA, Konradt C, Wojno EDT, Norose K, et al. Generalized Lévy walks and the role of chemokines in migration of effector CD8+ T cells. Nature. 2012;486(7404):545–548.

29. Ariotti S, Beltman JB, Borsje R, Hoekstra ME, Halford WP, Haanen JBAG, et al. Subtle CXCR3-dependent chemotaxis of CTLs within infected tissue allows efficient target localization. The Journal of Immunology. 2015;195(11):5285–5295.

30. Halle S, Keyser KA, Stahl FR, Busche A, Marquardt A, Zheng X, et al. In Vivo Killing Capacity of Cytotoxic T Cells Is Limited and Involves Dynamic Interactions and T Cell Cooperativity. Immunity. 2016;44(2):233–245. doi:10.1016/j.immuni.2016.01.010.

31. Mrass P, Oruganti SR, Fricke GM, Tafoya J, Byrum JR, Yang L, et al. ROCK regulates the intermittent mode of interstitial T cell migration in inflamed lungs. Nature communications. 2017;8(1):1–14.

32. Zhang X, Tan Y, Ling Y, Lu G, Liu F, Yi Z, et al. Viral and host factors related to the clinical outcome of COVID-19. Nature. 2020;doi:10.1038/s41586-020-2355-0.

33. Wölfel R, Corman VM, Guggemos W, Seilmaier M, Zange S, Müller MA, et al. Virological assessment of hospitalized patients with COVID-2019. Nature. 2020;doi:10.1038/s41586-020-2196-x.

34. Regan J, Flynn JP, Rosenthal A, Jordan H, Li Y, Chishti R, et al. Viral Load Kinetics of SARS-CoV-2 In Hospitalized Individuals with COVID-19. In: Open Forum Infectious Diseases; 2021.

35. Wiebe BM, Laursen H. Lung morphometry by unbiased methods in emphysema: bronchial and blood vessel volume, alveolar surface area and capillary length. Apmis. 1998;106(1-6):651–656.

36. Hart WS, Maini PK, Thompson RN. High infectiousness immediately before COVID-19 symptom onset highlights the importance of continued contact tracing. Elife. 2021;10:e65534.

37. Tindale LC, Stockdale JE, Coombe M, Garlock ES, Lau WYV, Saraswat M, et al. Evidence for transmission of COVID-19 prior to symptom onset. Elife. 2020;9:e57149.

38. Gandhi M, Beyrer C, Goosby E. Masks do more than protect others during COVID-19: reducing the inoculum of SARS-CoV-2 to protect the wearer. Journal of general internal medicine. 2020;35(10):3063–3066.

39. Yeh HC, Schum GM. Models of human lung airways and their application to inhaled particle deposition. Bulletin of Mathematical Biology. 1980;42(3):461–480. doi:https://doi.org/10.1016/S0092-8240(80)80060-7.

40. Kalimuddin S, Tham CYL, Qui M, de Alwis R, Sim JXY, Lim JME, et al. Early T cell and binding antibody responses are associated with Covid-19 RNA vaccine efficacy onset. Med. 2021;.

41. Cevik M, Tate M, Lloyd O, Maraolo AE, Schafers J, Ho A. SARS-CoV-2, SARS-CoV, and MERS-CoV viral load dynamics, duration of viral shedding, and infectiousness: a systematic review and meta-analysis. The Lancet Microbe. 2020;.

42. Bauer AL, Beauchemin CAA, Perelson AS. Agent-based modeling of host–pathogen systems: The successes and challenges. Information sciences. 2009;179(10):1379–1389.

43. Fricke GM, Letendre KA, Moses ME, Cannon JL. Persistence and adaptation in immunity: T cells balance the extent and thoroughness of search. PLoS Computational Biology. 2016;12(3):e1004818.

44. Xavier MP, Reis RF, dos Santos RW, Lobosco M. A simplified model of the Human Immune System response to the COVID-19. In: 2020 IEEE International Conference on Bioinformatics and Biomedicine (BIBM). IEEE; 2020. p. 1311–1317.

45. Ni L, Cheng ML, Feng Y, Zhao H, Liu J, Ye F, et al. Impaired cellular immunity to SARS-CoV-2 in severe COVID-19 patients. Frontiers in immunology. 2021;12.

46. Lucas C, Wong P, Klein J, Castro TBR, Silva J, Sundaram M, et al. Longitudinal analyses reveal immunological misfiring in severe COVID-19. Nature. 2020;584(7821):463–469.

47. Hickman HD, Reynoso GV, Ngudiankama BF, Cush SS, Gibbs J, Bennink JR, et al. CXCR3 chemokine receptor enables local CD8+ T cell migration for the destruction of virus-infected cells. Immunity. 2015;42(3):524–537.

48. Shan F, Gao Y, Wang J, Shi W, Shi N, Han M, et al. Abnormal lung quantification in chest CT images of COVID-19 patients with deep learning and its application to severity prediction. Medical physics. 2021;48(4):1633–1645.

49. Moses ME, Cannon JL, Gordon DM, Forrest S. Distributed adaptive search in T cells: lessons from ants. Frontiers in immunology. 2019;10:1357.

50. Levy R, Hill DB, Forest MG, Grotberg JB. Pulmonary fluid flow challenges for experimental and mathematical modeling; 2014.

51. Looney MR, Thornton EE, Sen D, Lamm WJ, Glenny RW, Krummel MF. Stabilized imaging of immune surveillance in the mouse lung. Nature Methods. 2011;8(1):91–96. doi:10.1038/Nmeth.1543.

52. Schneider M, Ackermann K, Stuart M, Wex C, Protzer U, Schätzl HM, et al. Severe Acute Respiratory Syndrome Coronavirus Replication Is Severely Impaired by MG132 due to Proteasome-Independent Inhibition of M-Calpain. Journal of Virology. 2012;86(18):10112–10122. doi:10.1128/JVI.01001-12.

53. Ganusov VV, De Boer RJ. Estimating In Vivo Death Rates of Targets due to CD8 T-Cell-Mediated Killing. Journal of Virology. 2008;82(23):11749–11757. doi:10.1128/JVI.01128-08.

54. Bar-On YM, Flamholz A, Phillips R, Milo R. SARS-CoV-2 (COVID-19) by the numbers. 2020;9:e57309. doi:10.7554/eLife.57309.

55. Miao H, Hollenbaugh JA, Zand MS, Holden-Wiltse J, Mosmann TR, Perelson AS, et al. Quantifying the early immune response and adaptive immune response kinetics in mice infected with influenza A virus. J Virol. 2010;84(13):6687–6698. doi:10.1128/JVI.00266-10.

56. Mohn KGI, Brokstad KA, Islam S, Oftung F, Tøndel C, Aarstad HJ, et al. Early Induction of Cross-Reactive CD8+ T-Cell Responses in Tonsils After Live-Attenuated Influenza Vaccination in Children. The Journal of Infectious Diseases. 2020;221(9):1528–1537. doi:10.1093/infdis/jiz583.

57. Powell T, Peng Y, Berthoud T, Blais ME, Lillie P, Hill A, et al. Examination of Influenza Specific T Cell Responses after Influenza Virus Challenge in Individuals Vaccinated with MVA-NP+M1 Vaccine. PloS one. 2013;8:e62778. doi:10.1371/journal.pone.0062778.

58. Keating R, Morris MY, Yue W, Reynolds CE, Harris TL, Brown SA, et al. Potential killers exposed: tracking endogenous influenza-specific CD8+ T cells. Immunology & Cell Biology. 2018;96(10):1104–1119. doi:https://doi.org/10.1111/imcb.12189.

59. Zheng Y, Kamil A, Driscoll MB, Shan H, Yelick K; IEEE. UPC++: a PGAS extension for C++. 2014; p. 1105–1114.